ACS APPLIED MATERIALS & INTERFACES

Research Article

Cite This: ACS Appl. Mater. Interfaces 2020, 12, 2023−2038

www.acsami.org

Moist-Retaining, Self-Recoverable, Bioadhesive, and Transparent in Situ Forming Hydrogels To Accelerate Wound Healing

Jun Li,[†] Fan Yu,[‡] Gong Chen,[§] Jia Liu,[∥] Xiao-Long Li,[⊥] Biao Cheng,[†] Xiu-Mei Mo,*[,‡] Cheng Chen,*[,§] and Jian-Feng Pan*[,†]

[†]Department of Orthopedics, Shanghai Tenth People's Hospital Affiliated to Tongji University, 301 Yanchang Road, Shanghai 200072, China

[‡]State Key Laboratory for Modification of Chemical Fibers and Polymer Materials, College of Chemistry, Chemical Engineering and Biotechnology, Donghua University, 2999 North Renmin Road, Shanghai 201620, China

[§]School of Environmental and Materials Engineering, College of Engineering, Shanghai Polytechnic University, Shanghai 201209, China

[∥]Department of Orthopedics, Shidong Hospital of Yangpu District, 999 Shiguang Road, Shanghai 200438, China

[⊥]Department of Orthopedics, Changhai Hospital, Naval Military Medical University, Shanghai 200433, China

Supporting Information

ABSTRACT: In the management of accelerating wound healing, moist environments play an important role. Compared with other scaffolds of various forms, hydrogels can maintain a moist environment in the wound area. They are cross-linked hydrophilic polymeric networks that resemble natural soft tissues and extracellular matrices. Among them, injectable hydrogels have attracted great attention in wound repair, as they can be injected into irregular-shaped skin defects and formed in situ to shape the contour of different dimensions. The excellent compliance makes hydrogels easy to adapt to the wound under different conditions of skin movement. Here, we oxidized hydroxyethyl starch (O-HES) and modified carboxymethyl chitosan (M-CMCS) to fabricate an in situ forming hydrogel with excellent self-recoverable extensibility−compressibility, biocompatibility, biodegradability, and transparency for accelerating wound healing. The oxidation degree of O-HES was 74%. The amino modification degree of M-CMCS was 63%. M-CMCS/O-HES hydrogels were formed through the Schiff base reaction. The physicochemical properties of M-CMCS/O-HES hydrogels with various ratios were investigated, and M-CMCS/O-HES hydrogel with a volume ratio of 5:5 exhibited appropriate gelation time, notable water-retaining capacity, self-recoverable conformal deformation, suitable biodegradability, and good biocompatibility for wound-healing application. Then, skin wound-healing experimental studies were carried out in Sprague−Dawley rats with full-thickness skin defects. Significant outcomes were achieved in the M-CMCS/O-HES hydrogel-treated group including higher wound closure percentage, more granulation tissue formation, faster epithelialization, and decreased collagen deposition. These findings demonstrate that using the obtained M-CMCS/O-HES hydrogels is a promising therapeutic strategy for wound healing.

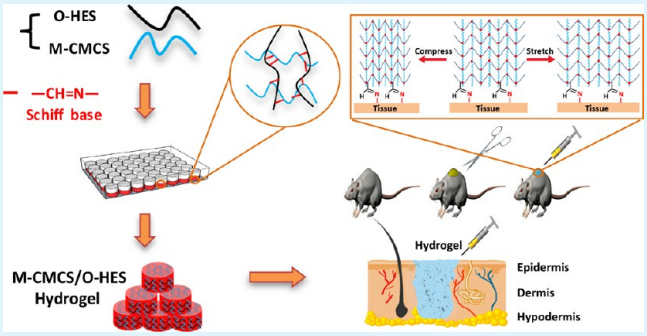

KEYWORDS: *injectable hydrogel, moisture retention, extensibility, compressibility, self-recovery, wound healing, skin regeneration*

1. INTRODUCTION

The skin covers the outer surface of the entire body, accounting for 8% of the total body mass. Its surface area varies with height and weight, and its thickness ranges from 1.5 to 4.0 mm. It forms an effective protective barrier between the body and the external environment, resisting the invasion of external pathogens.[1] Within a certain range, the skin also prevents damage from mechanical forces, chemicals, thermal burn, and ultraviolet radiation. Once the integrity of the skin is interrupted, there is a high probability of massive blood losses and microbial invasion, which can lead to catastrophic consequences.[2] Every year, a large number of patients die from multiple microbial infections and homeostatic imbalance that ensue when the skin defects are caused after traffic accidents, battlefield disasters, and other severe injuries.[3] For these patients, the prerequisites of the treatment are to accomplish the integrity of the skin and promote skin regeneration.[1] However, the lack of available natural skin substitutes makes it difficult for these patients with large skin defects.

Received: September 22, 2019
Accepted: December 19, 2019
Published: January 2, 2020

DOI: 10.1021/acsami.9b17180
ACS Appl. Mater. Interfaces 2020, 12, 2023−2038

Over the past decades, tissue engineering has been under way with steady progress. The technologies for preparing biomedical scaffolds and the functions and properties of biomaterials have also been investigated.[4] A variety of scaffolds, such as hydrogels,[5] electrospinning nanofibers,[6] gas-foaming sponges,[7] additive manufacturing composites,[8,9] and so forth, have been fabricated from natural or synthetic materials. Among them, hydrogels have been widely applied in tissue repair because of their high water content capacity and similarity to extracellular matrix (ECM). In the management of accelerating wound healing, a moist environment plays an important role.[10] Winter reported that wound healing was faster in a moist environment compared with a dry environment in the skin of young domestic pigs.[11] Then, Hinman and Maibach confirmed this moist wound care by using experimental human skin wounds.[12] Thus, hydrogels are superior to other scaffolds of various forms in wound-healing applications. In particular, in situ forming hydrogels can conform to the shape and size of different skin defects to restore the integrity of the skin.[13−15]

In daily life, the skin is not static. The topographic state of the skin changes with the movement of joints, limbs, and muscles. The hydrogel with excellent compliance makes it easy to adapt to the wound under different conditions. Traditional hydrogels with mechanical weakness and brittleness are often severely limited in many of such applications because their intrinsic mismatch mechanics results in interface failure under mechanical deformation in the skin including bending, twisting, stretching, and compression. Up to now, many efforts have been dedicated to developing self-adjustable hydrogels with rapid self-healing, extensibility, and compressibility, which are promising as soft tissue substitutes and tissue adhesives for skin wound healing.[16−18] The method of single dynamic covalent bonds (Schiff base) has also been employed to prepare hydrogels with desirable self-healing property for other applications.[19,20] Thus, the purpose of this study is to establish a transparent and in situ forming hydrogel with desirable moist-retaining, self-recoverable, extensible−compressible, and bioadhesive properties to accelerate wound healing.

During the process of wound healing, the essential requirement is the complete degradation of scaffolds to match the rate of tissue regeneration. The main advantage of natural over synthetic materials is the faster complete biodegradability and better biocompatibility. Natural biodegradable and biocompatible materials include polysaccharides, peptides, proteins, enzymes, polyphosphates, ribonucleic acids, and so on. Natural polysaccharides can be completely degraded and catabolized into carbon dioxide and water in vivo, including starch, cellulose, chitosan, sodium alginate, and more. Among them, chitosan, because of its nontoxicity, biocompatibility, biodegradability, antibacterial effect, and low cost, has been widely exploited as different formulations for tissue regeneration applications.[21,22] Especially in wound healing, chitosan-based injectable hydrogels exhibited conductive, antibacterial, and antioxidant effects to promote skin regeneration,[23,24] but the in vitro and in vivo hydrolysis results showed that the degradability of chitosan is slow and uncontrollable.[25] Compared with chitosan, carboxymethyl chitosan (CMCS) possesses much higher and controllable degradation rate after lysozyme treatment in vitro since the −COOH group accelerates the dissolution of CMCS.[26,27] Normally, wound healing needs to go through angiogenesis, granulation tissue formation, and epithelialization and is completed within several weeks after the injury.[28] Thus, CMCS with higher degradation rate than chitosan was chosen as a component in our study. Meanwhile, after grafting amino on CMCS, the interaction of positive and negative charges ($-NH_3^+$, $-COO^-$) in CMCS solution was diminished, resulting in superior solubility and solution fluidity of M-CMCS solution that is in favor of injectability. Moreover, the amino group is versatile and can function as a chemical cross-linking site for in situ forming hydrogels.

The significant advantage of in situ forming hydrogels over others is that the gel system can take an irregular shape of the skin defects. This requires that the precursor solutions must be injectable and then gelatinize in vitro or in vivo under appropriate conditions. Depending on the mechanism of preparation, hydrogels can be classified into physical and chemical cross-linking categories. The methods of triggering in situ gelation include Schiff-based reaction, Michael addition, photoinitiated polymerization, click chemistry cross-linking, ionic cross-linking, self-assembling gelation, and temperature responsive gelling. Among them, the reaction conditions and requirements for preparing Schiff-based hydrogels are mild and simple. The process can be carried out without adding additional cross-linking agents and initiators. It refers to the reaction between carbonyl groups and amino groups, generating imine groups (−C═N−). With the exception of the $-NH_2$ group in CM-chitosan as a cross-linking site, carbonyl groups of aldehyde polysaccharides have been employed as a component in Schiff-based hydrogels. The adjacent hydroxyl groups in the glucose unit of polysaccharides can be oxidized and cleaved by a strong oxidizing agent to obtain a product having an aldehyde structure. Thus, hydroxyethyl starch (HES), which is known to be low cost, low toxic, biocompatible, biodegradable, and abundant in nature, was employed as a component in our study.

In this study, we tested the feasibility of preparing an injectable hydrogel derived from CMCS and HES to facilitate wound healing. CMCS has chemically versatile amino and carboxyl groups. The carboxyl group on the molecular chain of CMCS was modified by ethylenediamine (ED) in the presence of 1-ethyl-3-(3-dimethyl laminopropyl) carbodiimide hydrochloride (EDC), and the carboxyl group was consumed to obtain an amino group. After that, the amino group on the modified CMCS (M-CMCS) was increased, and the carboxyl group was decreased. Thereby, the intermolecular forces between amino and carboxyl groups would be weakened, resulting in the increased fluidity of M-CMCS solution at room temperature. The amino content of M-CMCS was determined by the trinitrobenzenesulfonic acid (TNBS) method. HES was oxidized by sodium periodate, and the neighboring hydroxyl groups in the glucose ring of HES were broken to convert into dialdehyde groups. Hydroxylamine hydrochloride titration method was carried out to confirm the content of aldehyde group in oxidized HES (O-HES). Then, Schiff-based reaction between carbonyl groups and amino groups occurred to form an in situ cross-linking hydrogel through mixing M-CMCS and O-HES solutions together. The physicochemical properties and cytocompatibility of the hydrogel with different ratios of M-CMCS/O-HES were investigated to optimize the hydrogel components. Scanning electron microscopy (SEM) was used to observe the morphology, and the self-recoverable compliance property was verified by the conformal deformation measurement in the skin defects in vivo. The cytotoxicity and biocompatibility were further characterized by seeding with

DOI: 10.1021/acsami.9b17180
ACS Appl. Mater. Interfaces 2020, 12, 2023−2038

bone marrow-derived mesenchymal stem cells (BMSCs) in vitro and injecting subcutaneously in vivo. Through these assessments, the best formulated mixture condition was determined and then applied to enhance wound healing in a full-thickness skin defect model of Sprague−Dawley (SD) rats. These results showed that the hydrogel composed of M-CMCS/O-HES exhibited desirable physicochemical properties and significantly enhanced the regeneration of epidermis and controlled the collagen deposition in skin defects.

2. EXPERIMENTAL SECTION

2.1. Materials. CMCS (molecular weight of 200 kDa) with a substitution degree of 90% and a deacetylation degree of 82% was purchased from Bangcheng Chemical Co., Ltd. (Shanghai, China). HES (molecular weight of 130 kDa) with a substitution degree of 40%, sodium periodate, ED, and chloral hydrate were purchased from Sigma-Aldrich (St. Louis, MO, USA). EDC was purchased from GL Biochem Corporation (Shanghai, China). Fetal bovine serum, Dulbecco's modified Eagle's medium (DMEM), phosphate-buffered saline (PBS), and other reagents were purchased from Gibco Life Technologies Corporation (Carlsbad, CA, USA). CCK-8 was purchased from Dojindo Corporation (Kumamoto, Japan).

2.2. Synthesis of O-HES. O-HES was prepared from HES and sodium periodate according to the previous method. HES (10 g) was dissolved in deionized water by a magnetic stirring instrument to achieve 100 mL of HES solution. A certain amount of sodium periodate was dissolved in deionized water to get 10% (w/v) $NaIO_4$ solution. The prepared sodium periodate solution was placed in a separatory funnel and slowly added into HES solution drop by drop. The reaction solution was shielded from light and stirred at room temperature for 4 h and then terminated by adding 2 mL of ethylene glycol. After that, the reaction solution was dialyzed and purified in deionized water. The deionized water was changed four times per day till the dialyzate was periodate and ethylene glycol free. Then, the solution was lyophilized to obtain the product, O-HES. The oxidation degree (OD) of O-HES was determined by the hydroxylamine hydrochloride titration method. OD was defined as the molar ratio of the oxidized-opened aldose unit to the total HES glucopyranose ring monomer unit.

2.3. Synthesis of M-CMCS. CMCS (10 g) was uniformly dissolved in 400 mL of sodium dihydrogen phosphate solution (0.1 mol/L) by a magnetic stirring instrument to achieve a homogenous CMCS solution. Then, ED was added, and the pH of the solution was adjusted to 5.0 by adding hydrochloric acid. After that, EDC was added into the reaction solution. The reaction system was stirred with a magnetic stirrer at 37 °C for 6 h. The reaction mixture was then poured into a dialysis bag and dialyzed in deionized water for at least 3 days to purify the solution. The deionized water was changed four times per day till the dialyzate was ED and EDC free. Finally, the product was lyophilized to obtain M-CMCS and sealed for storage. The modification degree (MD) was calculated from the change of amino group content before and after chemical modification. The amino group in M-CMCS reacted with TNBS, and then the content of the amino group was determined by measuring the specific absorption peak of reaction products in the ultraviolet absorption spectrum. MD was defined as the ratio of the increased amino group content to the total carboxyl group content of CMCS. After chemical modification, the flow property of CMCS and M-CMCS solution was compared at room temperature using a vial tilting approach.

2.4. Preparation of M-CMCS/O-HES Hydrogel and Gelation Time Measurement. M-CMCS/O-HES hydrogel was prepared and used in wound healing. Gelation time was measured at 37 °C. O-HES solution was prepared at the concentration of 10% (w/v), and M-CMCS solution was prepared at the concentration of 5% (w/v) in a 37 °C water bath. Then, O-HES and M-CMCS solutions were injected into a transparent glass bottle in the ratio of 3/7, 4/6, 5/5, 6/4, and 7/3 and placed in a constant temperature oscillator at 37 °C. The oscillation frequency was 20 rpm. While the hydrogel gelled, no flow was observed during tilting the glass bottle. The gelation time was defined as the time from the mix of M-CMCS and O-HES to no flow observed in the glass bottle.

2.5. Swelling Performance Test of M-CMCS/O-HES Hydrogel. M-CMCS/O-HES solution was injected into a 48-well cell culture plate to prepare cylindrical hydrogel samples with the height of 4 mm. The samples were completely immersed in deionized water overnight at 37 °C to get a swelling equilibrium. Then, the surface of hydrogel samples was sufficiently blotted and accurately weighed in an electronic balance to record as W_1. After that, the samples were frozen at −80 °C and lyophilized in an ultralow temperature freeze dryer. The mass was accurately weighed and recorded as W_2. The degree of swelling (Q) was calculated according to the following formula: $Q = (W_1 - W_2)/W_2$, where W_1 is the mass of the hydrogel after reaching the swelling equilibrium and W_2 is the mass of the hydrogel after freeze drying.

2.6. Morphological and Structural Characterization of M-CMCS/O-HES Hydrogel. M-CMCS/O-HES hydrogel was prepared in a 48-well cell culture plate. The samples were frozen and lyophilized by using an ultralow temperature freeze dryer. The lyophilized samples were sliced and coated with gold for 120 s. Then, the samples were placed under a scanning electron microscope with an accelerating voltage of 5 kV to observe the morphological structure and internal porous conditions. The SEM images were collected, and pore diameters were statistically analyzed by using image analysis software (ImageJ, National Institutes of Health, USA).

2.7. Hydrolytic Degradation Properties of M-CMCS/O-HES Hydrogel. The samples were completely immersed in deionized water overnight at 37 °C to get a swelling equilibrium and accurately weighed as W_I. Subsequently, the samples were submerged in PBS solution containing 0.02% (w/v) sodium azide and placed in a shaker at 37 °C for time-dependent degradation study. On days 1, 3, 5, 7, and 14, the samples were taken out, and the moisture on the surface of the hydrogel sample was blotted with a filter paper. The mass of the hydrogel sample at this time was weighed and recorded as (W_t). The weight loss ratio of hydrogel because of degradation over time was calculated according to the following formula: weight loss ratio = $(W_I - W_t)/W_I$, where W_I is the initial mass of the hydrogel after reaching the swelling equilibrium and W_t is the remaining mass of the hydrogel after different time interval degradation over time.

2.8. Cell Viability and Proliferation of BMSCs Cocultured with M-CMCS/O-HES Hydrogel in Vitro. Cell viability and proliferation of BMSCs were assessed by coculturing with M-CMCS/O-HES hydrogel to evaluate the cytotoxicity in vitro. First, the bone marrow of SD rats was collected aseptically after anesthesia with 10% chloral hydrate (350 mg/kg). All animal experiments in this study were performed in accordance with the guidelines approved by the animal committee of the Tongji University, China. The collected bone marrow was dispersed in DMEM solution and centrifuged at 1500 rpm for 5 min to remove the supernatant. The remaining bone marrow was resuspended in complete medium and cultured in a 5% CO_2 incubator at 37 °C. The complete medium was replaced every 3 days to remove floating cells. The attached cells proliferated as primary BMSCs. When BMSCs reached 90% confluence after 7−10 days of primary culture, the cells were digested and subcultured in the ratio of 1:3 as passage 1. Then, M-CMCS/O-HES hydrogels were prepared in the 24-well tissue culture plates and seeded with BMSCs at a density of 5×10^4 cells mL^{-1}. The complete medium was changed every day. On days 1, 3, 7, and 14, the cell viability and proliferation of BMSCs were assessed through the CCK-8 assay. The culture medium containing CCK-8 reaction solution was added and incubated for 4 h at 37 °C under light shielding conditions. Then, 100 μL of the supernatant was transferred to a 96-well culture plate. The optical density value of absorbance at 450 nm was read using a multidetection microplate reader (MK3, Thermo, USA). The experiment was performed in triplicate, and the results reflected the condition of BMSCs proliferation. Meanwhile, after 7 days of culture, BMSCs were stained with phalloidine and 4′,6-diamidino-2-phenylindole (DAPI) to observe cell adhesion and spreading on hydrogel surfaces.

DOI: 10.1021/acsami.9b17180
ACS Appl. Mater. Interfaces 2020, 12, 2023−2038

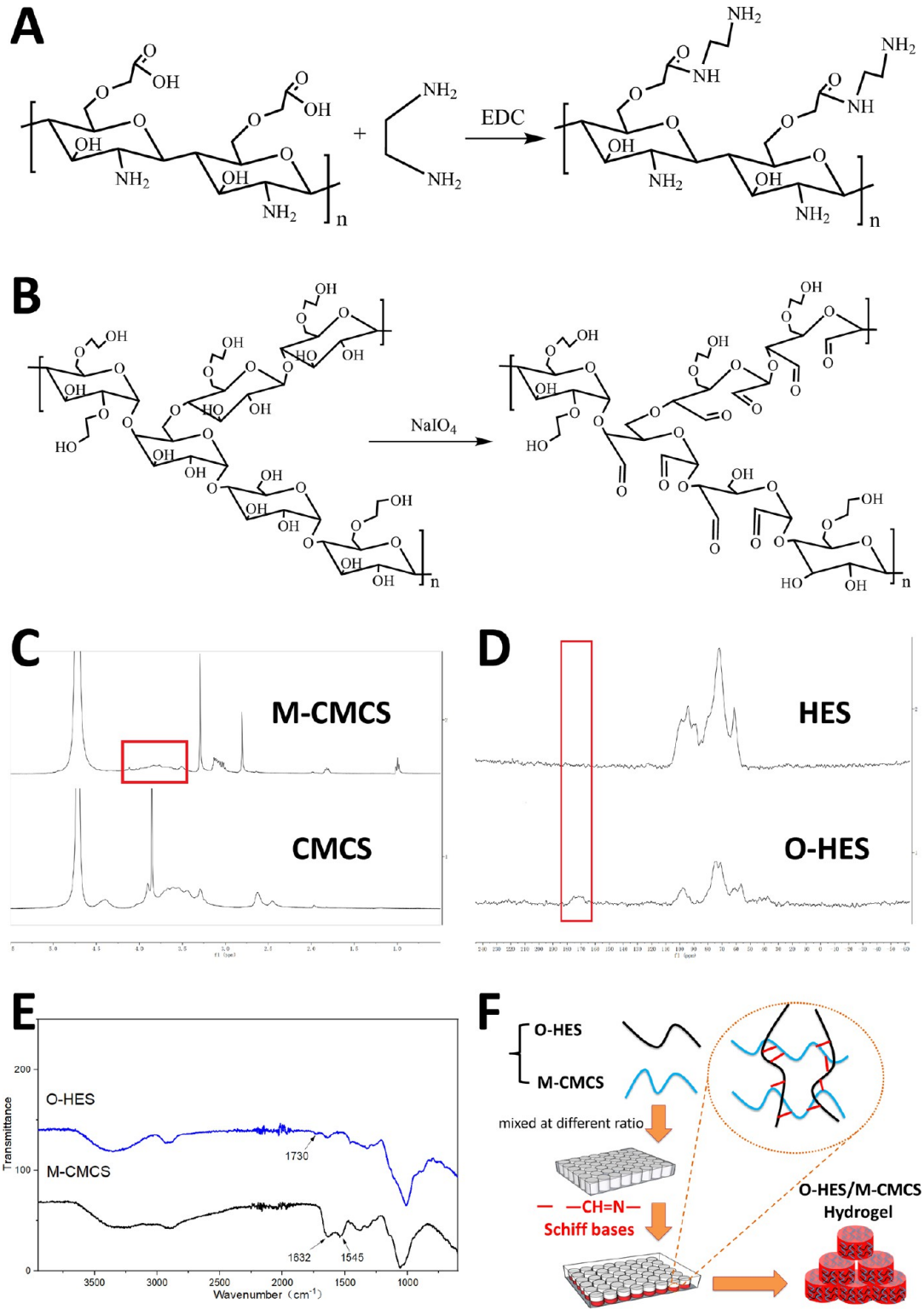

Figure 1. (A) Synthesis of M-CMCS to get more amino groups. (B) Synthesis of O-HES to introduce aldehyde groups. (C) ^{1}H NMR spectra of M-CMCS and CMCS. (D) ^{13}C NMR spectra of O-HES and HES. (E) FTIR spectra of M-CMCS and O-HES. (F) Mechanism for preparing M-CMCS/O-HES hydrogels through imine linkage.

2.9. Biocompatibility and Biodegradation Evaluation of M-CMCS/O-HES Hydrogel in Vivo. Biocompatibility measurement in vivo was performed by injecting M-CMCS/O-HES hydrogels subcutaneously into the dorsa of SD rats. After 1, 2, and 4 weeks, SD rats were sacrificed by overdose anesthetization, and the subcutaneous samples were harvested to assess local biocompatibility and biodegradation in vivo. Then, the vital organs were harvested including heart, liver, spleen, lung, and kidney to evaluate the systemic toxicity of M-CMCS/O-HES hydrogels. All samples were fixed in neutral buffered paraformaldehyde and embedded in paraffin. After that, they were sectioned and stained with hematoxylin and eosin (H&E) for histological observation. The animal experiments were approved by the animal committee of the Tongji University, China.

DOI: 10.1021/acsami.9b17180
ACS Appl. Mater. Interfaces 2020, 12, 2023−2038

2.10. Self-Recoverable Conformal Deformation Property of M-CMCS/O-HES Hydrogel. Self-recoverable conformal deformation property of M-CMCS/O-HES hydrogel was evaluated by injecting the hydrogel into the skin defects in vivo to verify the compliance of M-CMCS/O-HES hydrogel. Three circular defects of full-thickness skin were made in SD rats. After injection of M-CMCS/O-HES hydrogel, a horizontal or vertical force was applied in the surrounding skin to stretch and compress the wound. In the stretching and compression states, the dimension of wound area was measured. The conformal deformation was calculated according to the following formula: deformation = D_1/D_0, where D_1 is the dimension of the wound after reaching the extension or compression state and D_0 is the dimension of the initial shape of the wound.

Then, the mechanical property of the adhesive strength on soft tissues was determined by stretching the overlapped skin stuck by M-CMCS/O-HES hydrogel. The bonding tensile strength was measured by using a Dejie DXLL-20000 material testing instrument at a testing rate of 10 mm/min. Commercial fibrin glue was used and compared under the same condition.

2.11. Skin Wound Healing with M-CMCS/O-HES Hydrogel in SD Rats. Twenty-four healthy male SD rats (6−8 weeks old, weighing 250−300 g) were selected for skin wound-healing experimental studies. After anesthetization with 10% chloral hydrate, two 1.5 cm diameter circular defects of full-thickness skin with a 5 cm interval were made by using a surgical scissors instrument on the dorsum of each rat. The upper skin defects were treated with M-CMCS/O-HES hydrogel, and the lower skin defects were not treated with any material as the control group. The morphologies of the wounds and the conditions of healing process were observed immediately after surgery, 3, 7, 14, and 21 days after treatment.

2.12. Wound-Healing Analysis. During the process of wound healing, the percentage of wound closure was calculated to assess the difference in healing rates treated with M-CMCS/O-HES hydrogel or not. Briefly, all rats on days 3, 7, 14, and 21 after surgery were anesthetized and placed against the backdrop of a metric ruler. High-resolution images were captured from the wound and analyzed by using ImageJ software. The wound area was measured by the limits of grossly evident epithelialization.

The percentage of wound closure was calculated by

$$\text{Wound closure percentage } (\%) = (A_1 - A_2/A_1) \times 100\%$$

where A_1 is the area of original wound after surgery and A_2 is the area of wound on days 3, 7, 14, and 21 after surgery.

2.13. Histological Analysis. On days 3, 7, 10, 14, and 21 after surgery, the rats were sacrificed, and the wound samples together with a surrounding rim of normal skin were harvested. For histological analysis, the samples were first fixed in 4% neutral buffered paraformaldehyde, sequentially dehydrated in a series of ethanol with increasing gradient concentration, and cleared by the exposure to xylene. Then, the samples were incubated with paraffin−xylene solution in an oven overnight, to remove the xylene, and embedded in paraffin. The paraffin-embedded samples were sectioned at the thickness of 8.0 μm to adhere to glass slides. After the process of dewaxing and hydration, the sections were stained with H&E for routine examination. Then, Masson's trichrome staining was performed to further analyze the characteristics of these wound samples.

3. RESULTS

3.1. Fabrication and Characterization of O-HES, M-CMCS, and M-CMCS/O-HES Hydrogels. CMCS is an amphoteric water-soluble derivative of chitosan that exhibits enhanced water solubility, inherent biodegradability, excellent biocompatibility, and many other outstanding physicochemical and biological properties. In aqueous solution, CMCS can undergo both acid electrolysis and alkaline electrolysis. Therefore, CMCS solution contains both positive and negative charge groups. The intermolecular force between positive and negative charges results in poor solubility and solution fluidity. In this study, ED was grafted onto CMCS in the presence of EDC (Figure 1A). Theoretically, there is a probability of cross-linking of CMCS with ED to form a hydrogel. However, the reaction process goes on for 6 h at 37 °C by stirring with a magnetic stirrer. There was no probability of forming hydrogel directly. Moreover, the formation of hydrogel must be based on one ED molecule reacting with two CMCS molecules to form a network structure. In the reaction system, the molar ratio of ED to COOH was 20 to 1. The concentration of ED used in the reaction was absolutely higher than that of CMCS. The probability of one ED molecule cross-linking with two CMCS molecules is scarce. As a result, ED was grafted onto CMCS. Carboxyl groups of CMCS were consumed, and amino groups were grafted and increased in M-CMCS. Figure 1C shows the ^{1}H nuclear magnetic resonance (NMR) spectra of M-CMCS and CMCS. Compared with CMCS, there was a new peak appearing at 2.80 ppm in the ^{1}H NMR curve of M-CMCS. This was assigned to the methylene hydrogen signal of ED grafting onto CMCS. In the Fourier transform infrared spectroscopy (FTIR) curve of M-CMCS (Figure 1E), the peak appearing at 1632 cm^{-1} was associated with the C═O stretching vibration (amide I band) and the peak at 1545 cm^{-1} was associated with the N−H stretching vibration (amide II band). Thus, ED was successfully grafted onto CMCS. The mole of consumed carboxyl group was equivalent to the mole of grafted amino group. The MD of M-CMCS was 63%, indicating that 63% of carboxyl groups were converted into amino groups. The amino content of M-CMCS was measured as approximately 0.53 mmol g^{-1} by the TNBS method, showing that 1 g of M-CMCS contained 0.53 mmol amino group. After chemical modification, M-CMCS solution exhibited superior solubility and solution fluidity because of the diminished interaction of positive and negative charges in the solution. The concentration of M-CMCS solution used in this study is 5% (w/v), whereas the saturated concentration of CMCS solution usually is 3% (w/v).

HES is a nonionic starch derivative consisting of large amounts of glucose units linked by glycosidic bonds. Structurally, HES has a dendritic branch structure with a large relative molecular mass. The D-glucopyranose units are linked by α-1,4-glycosidic bonds in the linear chain, and branching chain takes place in the linear through α-1,6-glycosidic bonds. The hydroxyl groups of glucose units are located in C2, C3, and C6, wherein the adjacent hydroxyl groups of C2 and C3 can be oxidized by sodium periodate to introduce dialdehyde groups (Figure 1B). Figure 1D shows the ^{13}C NMR spectra of O-HES and HES. After oxidation reaction, there was a new peak appearing at 160−220 ppm in the ^{13}C NMR curve of O-HES. This was assigned to the signal of the C═O group, indicating that aldehyde groups were produced. Moreover, the peak appearing at 1730 cm^{-1} in the FTIR curve of O-HES was also assigned to the aldehyde group C═O stretching vibration, indicating that the oxidation reaction actually occurred (Figure 1E). In our study, HES was oxidized by sodium periodate with the OD of approximately 74% measured by reacting with hydroxylamine hydrochloride. This indicated that 74% of glucopyranose rings in HES were oxidized and cleaved to introduce aldehyde groups.

The solubility properties of O-HES and M-CMCS were attributed to the presence of hydrophilic functional groups of OH, COOH, CHO, and NH_2, which could be used for the formation of hydrogels. While O-HES and M-CMCS solutions

DOI: 10.1021/acsami.9b17180
ACS Appl. Mater. Interfaces 2020, 12, 2023−2038

were mixed together, covalent linkages (−C═N−) between these two polymer chains were established by the Schiff-based reaction of aldehyde groups and amino groups (Figure 1F). Because of these covalent cross-links, permanent junctions were created to form hydrogel polymeric networks. Compared with other chemical cross-linking methods, Schiff bases were formed under mild conditions. By changing the polymer volume fraction and the degree of cross-linking, many of the network properties could be controlled, including gelation time, swelling properties, porosity, pore size, and degradation of the hydrogels. The volume ratios of M-CMCS/O-HES for M-CMCS7/O-HES3, M-CMCS6/O-HES4, M-CMCS5/O-HES5, M-CMCS4/O-HES6, and M-CMCS3/O-HES7 were 7:3, 6:4, 5:5, 4:6, and 3:7, respectively.

3.2. Gelation Time of M-CMCS/O-HES Hydrogels with Various Ratios. Injectable hydrogels can be injected into irregular-shaped tissue defects because the precursor components of hydrogel are flowing solutions. Drugs and cells can be incorporated easily in the solution state of gel. While the cross-linking reaction occurred, the state of the hydrogel system converted from free-flowing liquid into a nonflowing gel to shape the contour of different dimensions. The gelation time is an important parameter for hydrogels. In this study, the gelation time of M-CMCS/O-HES hydrogels with various ratios was determined by using a constant temperature oscillator at 37 °C.

As for all formulated hydrogels, gelation time was significantly less than 30 s. When changing the polymer volume fraction of O-HES and M-CMCS, a different gelation time was achieved as shown in Figure 2. As the volume fraction

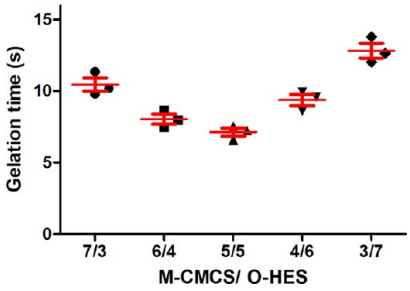

Figure 2. Gelation time of M-CMCS/O-HES hydrogels with various volume ratios measured at 37 °C.

of O-HES increased, the gelation time decreased first and then increased. From M-CMCS7/O-HES3 to M-CMCS5/O-HES5, the increase in O-HES allowed more aldehyde groups to cross-link with amino groups, resulting in shorter gelation time. Whereas O-HES was increased to a certain extent (M-CMCS5/O-HES5), the decrease in M-CMCS from M-CMCS5/O-HES5 to M-CMCS3/O-HES7 caused a decrease in the cross-linking reaction of aldehyde groups and amino groups, thereby resulting in longer gelation time. Thus, M-CMCS7/O-HES3 and M-CMCS3/O-HES7 exhibited longer gelation time than M-CMCS5/O-HES5. This was ascribed to the excess of M-CMCS or O-HES in the hydrogel precursor system.

3.3. Evaluation of Equilibrium Swelling and Water-Retaining Capacity of M-CMCS/O-HES Hydrogels. The equilibrium swelling of hydrogels is an important feature for their use in vivo as highly swollen hydrogels can absorb and retain large amounts of tissue fluids and nutrients. The excellent water-retaining capacity of hydrogels facilitates both cell attachment and penetration during the process of tissue regeneration. To explore their water-retaining capacity, we evaluated the time dependency of the swelling ratio and the equilibrium swelling of hydrogels. As shown in Figure 3A, the

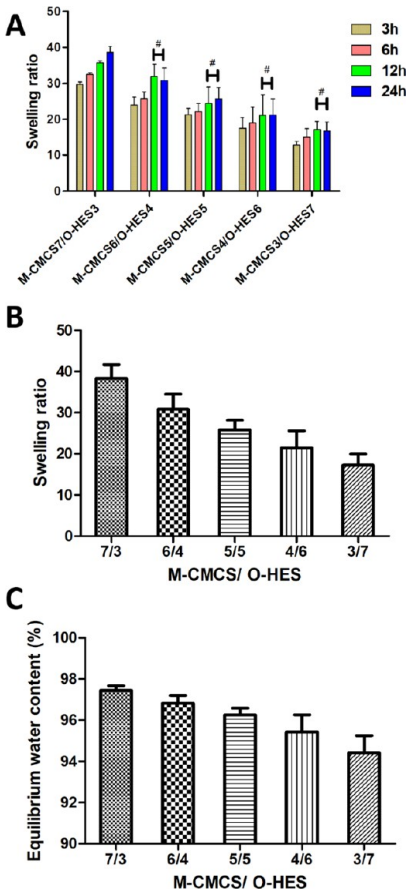

Figure 3. (A) Swelling ratio of M-CMCS/O-HES hydrogels with various volume ratios at different time points (# indicates that there was no significant difference). (B) Swelling ratio of M-CMCS/O-HES hydrogels with various volume ratios at equilibrium swelling state. (C) Equilibrium water content of M-CMCS/O-HES hydrogels with various volume ratios.

swelling ratio of hydrogels gradually increased with the time of immersion in deionized water. After 12 h, M-CMCS/O-HES hydrogels with the ratio of 6/4, 5/5, 4/6, and 3/7 reached the equilibrium swelling state. There was no significant difference between 12 and 24 h. Figure 3B,C shows the swelling ratio and equilibrium water content of lyophilized hydrogels in PBS. The M-CMCS/O-HES hydrogel had the swelling ratio in the range of 15−40 and equilibrium water content in the range of 94−98%.

As the volume fraction of O-HES increased, both the swelling ratio and equilibrium water content decreased gradually. Generally, the swelling ratio is dependent upon not only the degree of cross-linking but also the volume fraction of polymers. More density of cross-linking sites or volume fraction will make for lower swelling ratio. From M-CMCS7/O-HES3 to M-CMCS5/O-HES5, the increase in O-HES resulted in more cross-linking sites between aldehyde groups and amino groups. Then, from M-CMCS5/O-HES5 to M-CMCS3/O-HES7, the decrease in M-CMCS caused a

DOI: 10.1021/acsami.9b17180
ACS Appl. Mater. Interfaces 2020, 12, 2023−2038

decrease in the cross-linking reaction, whereas the volume fraction of O-HES increased, and the concentration of increased O-HES was higher than that of decreased M-CMCS. So, the swelling ratio decreased gradually from M-CMCS7/O-HES3 to M-CMCS3/O-HES7. Correspondingly, the equilibrium water content also decreased gradually indicating that the water-retaining capacity was also dependent upon the degree of cross-linking and the polymer volume fraction of O-HES and M-CMCS. Equilibrium water content of all formulated hydrogels was above 94%, suggesting that they could maintain significant amounts of body fluids in vivo.

3.4. Morphological Characteristics of M-CMCS/O-HES Hydrogels. Hydrogels are three-dimensional cross-linked networks of polymer chains. In the above study, they absorbed large amounts of water ranging from 15 to 40 times of their original weight. Lyophilized hydrogel samples were transversely sectioned and observed by using a scanning electron microscope to confirm their porosity and internal structure. Porosity is an important parameter for oxygen and nutrients to diffuse inside and outside the hydrogels. The transverse section of lyophilized hydrogel samples with various ratios is shown in Figure 4. Porosity completely penetrated throughout all hydrogel samples. They consisted of individual openings and interconnecting pores. Individual openings provided access and space for cell ingrowth. At the same time, interconnected pores enhanced the diffusion of nutrients from the surrounding area to the center of the hydrogel. This property qualified M-CMCS/O-HES hydrogels as suitable templates for guiding cell growth and tissue regeneration.

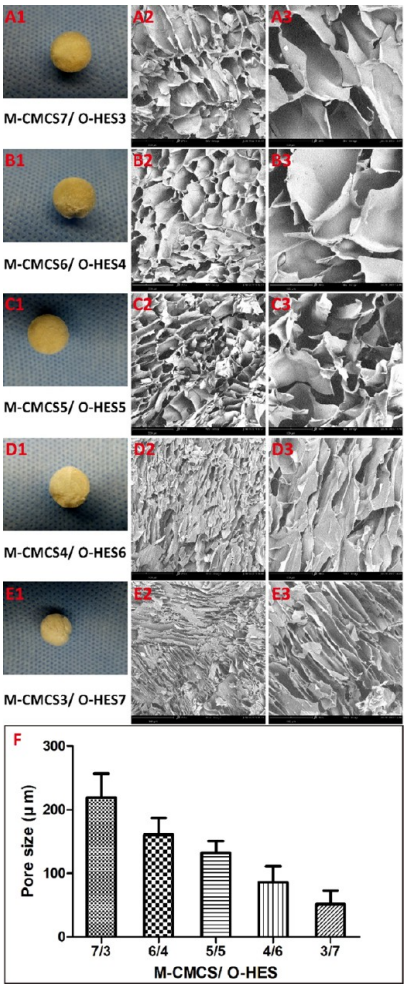

Figure 4. Gross view of M-CMCS/O-HES hydrogels (A1−E1) and SEM observation of lyophilized hydrogels with various volume ratios [scale bar 300 μm: (A2−E2); scale bar 100 μm: (A3−E3)]. (F) Pore size of M-CMCS/O-HES hydrogels with various volume ratios.

The porosity and pore size were also controlled by varying the volume ratios of M-CMCS and O-HES. The average pore size of M-CMCS/O-HES hydrogels depended on the density of chemical cross-linking as well as the polymer volume fraction of O-HES and M-CMCS. As shown in Figure 4F, the average pore size decreased gradually from M-CMCS7/O-HES3 to M-CMCS3/O-HES7. The statistical analysis showed that the pore size exhibited an obvious dependence on the ratio of M-CMCS/O-HES. The average pore diameters of M-CMCS7/O-HES3, M-CMCS6/O-HES4, and M-CMCS5/O-HES5 were more than 100 μm, whereas the average pore diameters of M-CMCS4/O-HES6 and M-CMCS3/O-HES7 decreased less than 100 μm. In order to ensure the tissue viable and healthy, it is necessary for the pores to be greater than 50−150 μm. Vascular tissue does not appear in pore sizes less than 100 μm. Suitable pore size required for tissue regeneration is due to the need to provide a blood supply to the ingrown connective tissue. Thus, in applications for wound healing, the adjustment of the pore structure to desired levels appears to be mandatory. This can be ensured by engineering the appropriate pore size distribution in the fabrication process of M-CMCS/O-HES hydrogels.

3.5. Cell Viability and Proliferation of BMSCs Cocultured with M-CMCS/O-HES Hydrogels in Vitro. To define the influence of M-CMCS/O-HES hydrogels on cell viability and proliferation, BMSCs were isolated from the bone marrow of SD rats and seeded on hydrogels with different volume ratios. We evaluated the cytocompatibility of M-CMCS/O-HES hydrogels through the CCK-8 assay. The cells cultured on the empty culture plate were considered as the control group, and the cell viability was showed as optical density. The higher value represented more cell viability. During the period of culturing time, BMSCs exhibited highly proliferative capacity in the empty culture plate and all hydrogel surfaces. As shown in Figure 5A, the number of viable cells in all groups increased with the culturing time, indicating that M-CMCS/O-HES hydrogels had no obvious harmful effect on BMSCs viability and proliferation.

The viability of BMSCs cultured on M-CMCS4/O-HES6 and M-CMCS3/O-HES7 was lower than that of M-CMCS7/O-HES3, M-CMCS6/O-HES4, and M-CMCS5/O-HES5 during the period of culturing time. This was due to the aldehyde groups of excessive O-HES in the hydrogel, which were unfavorable for cell viability and proliferation. On the first and third day, the viability of BMSCs cultured on M-CMCS5/O-HES5 exhibited no statistically significant difference from that of M-CMCS7/O-HES3 and M-CMCS6/O-HES4. However, after 7 and 14 days of culturing, the viability of BMSCs cultured on M-CMCS5/O-HES5 was higher than that of M-CMCS7/O-HES3 and M-CMCS6/O-HES4. This was due to the faster dissolution of M-CMCS7/O-HES3 and M-CMCS6/O-HES4 than M-CMCS5/O-HES5. Rapid degradation of hydrogel resulted in some extent of cell loss while changing complete medium every day. Thus, these results indicated that M-CMCS5/O-HES5 hydrogel exhibited better cell viability and proliferation performance than other formulated hydrogels.

DOI: 10.1021/acsami.9b17180
ACS Appl. Mater. Interfaces 2020, 12, 2023−2038

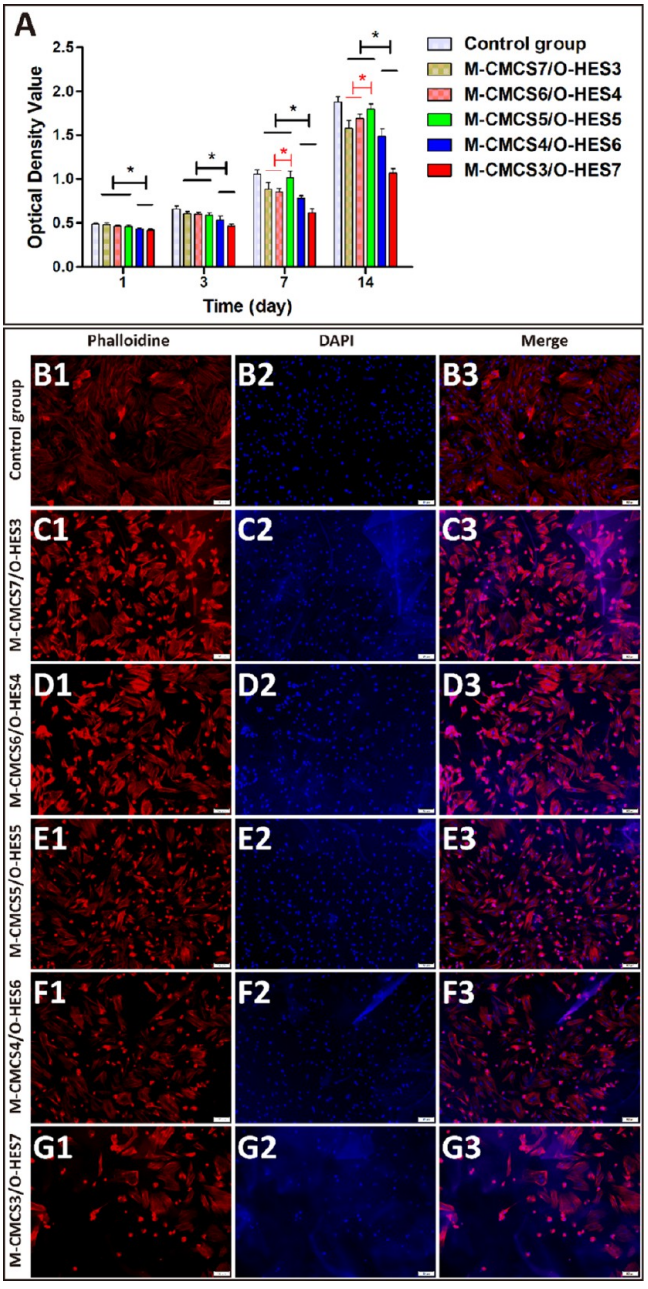

Figure 5. (A) Cell viability and proliferation of BMSCs cocultured with M-CMCS/O-HES hydrogels in vitro for 1, 3, 7, and 14 days. After 7 days of culture, the cytoplasm of BMSCs was stained with phalloidine (B1−G1) and cell nuclei were stained with DAPI (B2−G2) to further observe the cell morphology on a tissue culture plate (control group) and hydrogel surfaces [(B3−G3) are the merged images of (B1-G1) and (B2-G2)].

Then, the cytoplasms of BMSCs were stained with phalloidine and the cell nuclei were stained with DAPI to further observe the cell morphology on hydrogel surfaces. BMSCs cultured on the empty culture plate showed an elongated or spindle-shaped morphology, which closely resembles fibroblastic appearance. As illustrated in Figure 5B1, no round morphologies were seen on this surface, reflecting the fact that in this case, cytoplasms of BMSCs completely spread out over the surface of the culture plate. Moreover, the cell nuclei were stained as round by DAPI (Figure 5B2). Figure 5B3 was the merge of Figure 5B1,B2.

Although BMSCs were able to adhere, spread, and grow on hydrogel surfaces in vitro, the ability to support cell attachment or spreading was found to differ. From M-CMCS7/O-HES3 to M-CMCS3/O-HES7, hydrogel prevented the flattening out or spreading of BMSCs onto the surface. BMSCs spreading on M-CMCS3/O-HES7 surface are less extensive than those on M-CMCS7/O-HES3 surface, suggesting that with the increase of O-HES, the excess of aldehyde groups also prevented BMSCs from flattening out and spreading on hydrogel surfaces.

3.6. Biodegradability Measurement of M-CMCS/O-HES Hydrogels in Vitro and in Vivo. Resorbable scaffolds are designed and based on biological principles of repair that have evolved over millions of years. Natural tissues such as skin and soft tissue can repair and replace tissue-engineering scaffolds throughout the period of tissue regeneration. The degradation and resorption rates must be matched to the repair rates of body tissues to avoid too rapid or too slow dissolution.

The degradation of M-CMCS/O-HES hydrogels in vitro was assessed and is shown in Figure 6A. Apparently, the volume ratios of M-CMCS/O-HES had an important influence on the degradation rate of hydrogels. As the volume fraction of O-HES increased, the degradation rate decreased first and then increased. M-CMCS5/O-HES5 showed the lowest degradation rate and the highest weight remaining. The weight remaining increased from M-CMCS7/O-HES3 to M-CMCS5/O-HES5 and then decreased from M-CMCS5/O-HES5 to M-CMCS3/O-HES7. This phenomenon was in line with the result of gelation time, suggesting that the degree of Schiff-based cross-linking reaction influenced the degradation rate as well as the gelation time.

As M-CMCS/O-HES hydrogels were designed to accelerate wound healing, it was also essential to evaluate the biodegradability property in vivo. According to the above results, M-CMCS5/O-HES5 was formulated and injected subcutaneously into the dorsa of SD rats. The weight remaining of M-CMCS5/O-HES5 hydrogel decreased gradually over the period of degradation (Figure 6B). Over the first 2 weeks, the hydrogel degraded at a moderate rate, and the weight remaining was more than 50%. However, in the next 2 weeks, M-CMCS5/O-HES5 hydrogel showed fast degradation. After 4 weeks of degradation, the weight remaining of hydrogel was lower than 20% of the original weight. These results indicated that M-CMCS5/O-HES5 hydrogel had good biodegradability and can be replaced by regenerated tissue in the process of wound healing. Furthermore, Figure 6C showed the morphology of M-CMCS5/O-HES5 hydrogel after degradation in vivo. Compared with 1 week and 2 weeks, the remaining hydrogel was obviously thinner and smaller at 4 weeks. This biodegradability enabled M-CMCS5/O-HES5 hydrogel to be a suitable scaffold for wound healing.

3.7. Biocompatibility Measurement of M-CMCS/O-HES Hydrogels in Vivo. Resorbable hydrogels were designed to degrade gradually over a period of time in vivo and then were replaced by the natural host tissue. In biology, homeostasis is a sophisticated internal physical and chemical condition. Complex interactions between cells in body fluids and humoral components involve activators, effectors, receptors, inhibitors, and other regulators. These interactions produce aggressive immune responses to any foreign implanted scaffold through the processes of adhesion, chemical reaction, and particulate transport. In the test of biocompatibility measurement in vivo, two perspectives were considered for which a thorough evaluation of tissue compatibility was

DOI: 10.1021/acsami.9b17180
ACS Appl. Mater. Interfaces 2020, 12, 2023−2038

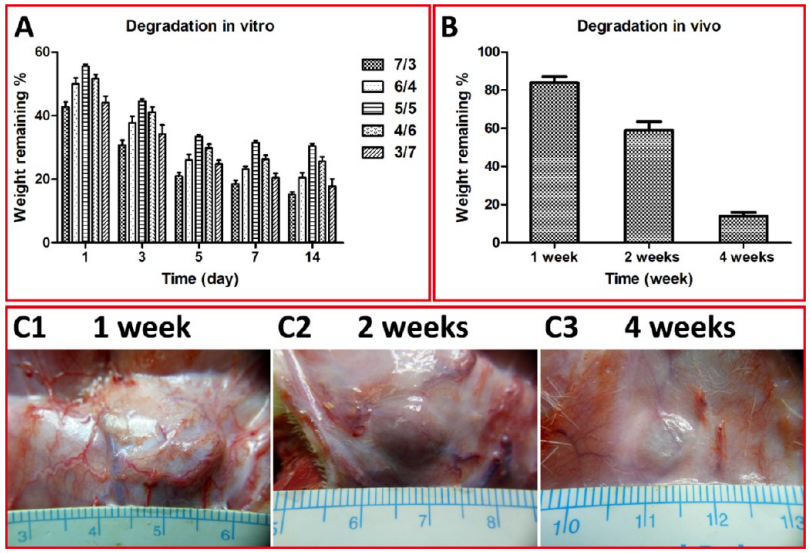

Figure 6. Biodegradability measurement of M-CMCS/O-HES hydrogels in vitro and in vivo. (A) In vitro degradation of M-CMCS/O-HES hydrogels with various volume ratios on days 1, 3, 5, 7, and 14. (B) In vivo degradation of M-CMCS5/O-HES5 hydrogel after subcutaneous injection into the dorsa of SD rats after 1, 2, and 4 weeks. (C) General observation of M-CMCS5/O-HES5 hydrogel after degradation in vivo.

necessary for further application and development. Thorough studies of tissue compatibility demanded both local and systemic measurements rather than just local assessment.

The first perspective involved the assessment of focal foreign-body reaction to determine the local biocompatibility of M-CMCS/O-HES hydrogels. As illustrated in Figure 7,

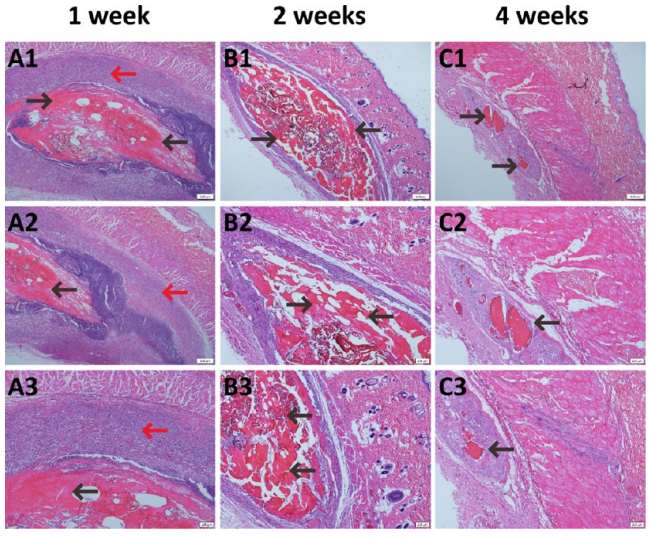

Figure 7. Local tissue compatibility measurement of M-CMCS/O-HES hydrogels in vivo after 1 week (A), 2 weeks (B), and 4 weeks (C) (black arrows: M-CMCS/O-HES hydrogels; red arrows: tissue interfacial thickness of immune responses to foreign materials.).

there was a very thin or nonexistent interfacial thickness between M-CMCS/O-HES hydrogel and the host tissue. This interfacial thickness of tissue was immune response to foreign materials. After subcutaneous injection into the dorsa of SD rats for 1 week, a thin interfacial thickness of tissue was observed and stained as basophilic by H&E (Figure 7A3). Compared with 1 week, the interfacial thickness of tissue between M-CMCS/O-HES hydrogel and the host tissue was thinner after 2 weeks and mainly disappeared after 4 weeks.

The second perspective regarding the in vivo biocompatibility assessment focused on the systemic toxicity of M-CMCS/O-HES hydrogels. The systemic toxicity evaluation determined the potential harmful effects of M-CMCS/O-HES hydrogels on vital organs in vivo that were away from the point of contact. After 1, 2, and 4 weeks of subcutaneous injection, all rats survived healthily, and no adverse effects were observed. Vital organs were estimated by histological staining including heart, liver, spleen, lung, and kidney. As presented in Figure 8, there was no tissue necrosis or inflammatory cell infiltration observed in these organs during the period of hydrogel degradation. The histological structures were normal, indicating that the constituents of M-CMCS/O-HES hydrogels released into the body did not produce organ dysfunction and systemic effects in vivo.

3.8. Self-Recoverable Compliance Property of M-CMCS/O-HES Hydrogel in Vivo. As presented in Figure 9 and Video S1 (Supporting Information 1), M-CMCS/O-HES hydrogel fitted well with the irregular shapes and accommodated the skin movement. During the extension and compression movement, the hydrogels stretched up to maximum 120% and compressed to minimum 55% to match various skin deformations. In the extension state, there was no fracture, whereas in the compression state, there was a small wrinkle present on the hydrogel (Figure 9A,B). When the external force was removed, the hydrogels restored their original shapes (Figure 9C). Reversible extension and compression of M-CMCS/O-HES hydrogel was observed and repeated many times (Figure 9D). There was no significant loss in the stretching and compression capacity. After 100 cycles of stretching and compression movement, M-CMCS/O-HES hydrogel still stuck to the natural tissue in the skin defects. These results indicated that M-CMCS/O-HES hydrogel exhibited excellent tissue-attachable property in the wound area. In the mechanical strength test, the adhesive strength of commercially available fibrin glue was 14.07 ± 1.15 kPa. The mechanical tensile strength of M-CMCS/O-HES hydrogel was 25.74 ± 1.95 kPa, which was higher than that of fibrin glue. The mechanism was that the incorporating functional groups of −CHO within the M-CMCS/O-HES

DOI: 10.1021/acsami.9b17180
ACS Appl. Mater. Interfaces 2020, 12, 2023−2038

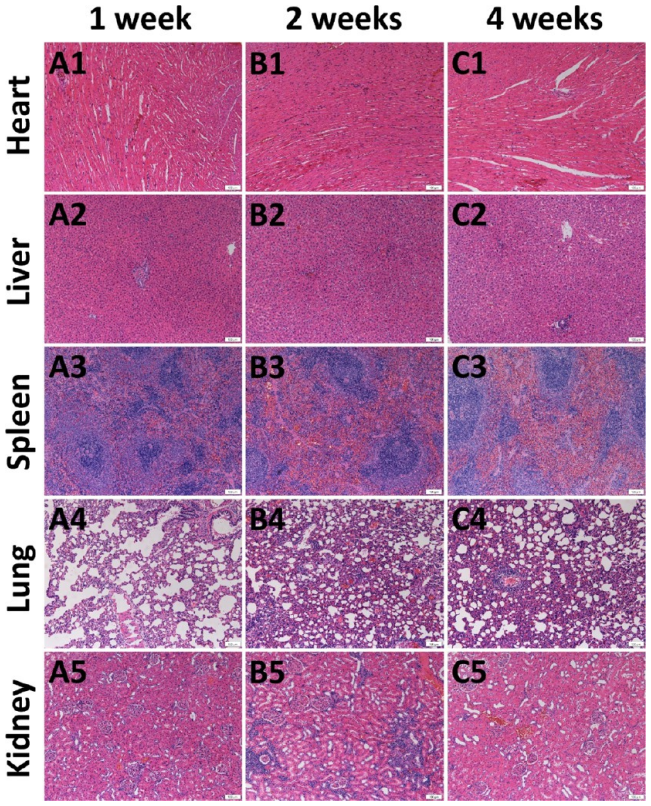

Figure 8. Systemic toxicity measurement of M-CMCS/O-HES hydrogels in vivo after 1 week (A), 2 weeks (B), and 4 weeks (C) through histological evaluation of heart, liver, spleen, lung, and kidney.

hydrogel interacted and bound with the surrounding tissue through imine linkage to mechanically stick the hydrogel in place (Figure 9E). Thus, the excellent compliance endowed M-CMCS/O-HES hydrogel with the ability to fit well with the skin movement under different states. M-CMCS/O-HES hydrogel was proved to strongly stick to the skin naturally by imine linkage with excellent conformal contact during various skin deformations.

3.9. Wound-Healing Effect of M-CMCS/O-HES Hydrogel for Full-Thickness Skin Defects in Vivo. Figure 10A showed that the full-thickness skin defects were filled with M-CMCS/O-HES hydrogel in the SD rat model to observe the effect of hydrogel on wound healing. Compared with the untreated control wounds, full-thickness skin defects treated with the hydrogel exhibited an accelerated wound closure. A quantitative analysis of wound closure was conducted, and the results showed that wound closure percentage in the M-CMCS/O-HES hydrogel group was significantly higher than that in the control group at all time points (Figure 10B). On day 21 after surgery, the wound was mainly healed in the M-CMCS/O-HES hydrogel group. These indicated that M-CMCS/O-HES hydrogel could be helpful in promoting skin regeneration. From the observation of the wound appearance, the skin defects treated with M-CMCS/O-HES hydrogel had faster healing rate at the early stages of healing process (3, 7, and 14 days after surgery). The faster closure rate of untreated wounds was mainly presented at the later stages of healing from day 14 to day 21 (Figure 10B,C).

Then, the histological analysis was performed by using H&E and Masson's trichrome staining. As observed from the H&E staining images of Figure 11, huge amounts of capillary vessels were clearly detected in both groups in the early stages of wound healing (3, 7, and 14 days). Compared with the control group, the angiogenic activity of M-CMCS/O-HES hydrogel was significantly higher (white arrows, Figure 11B1−B3 vs 11D1−D3). During the period of skin regeneration, the degree of neovascularization in both groups decreased with time (Figure 11B,D). We considered that the presence of more capillary vessels in the early stages of healing process provided more nutrients to promote skin regeneration, and then the degree of neovascularization decreased to a certain extent so as to maintain skin metabolism and stability. As a result, the amounts of capillary vessels increased in the M-CMCS/O-HES hydrogel group and subsequently promoted skin regeneration at the wound sites. After 21 days of skin regeneration, the epidermal layer was completely formed as shown by yellow arrows. Compared with the control group, there were more detectable skin appendages including hair follicles, sweat glands, sebaceous glands, nerve receptors, and vascular structures in the M-CMCS/O-HES hydrogel group (Figure 11B5,D5, black arrows). These structures made regenerated skin more similar to normal skin in the M-CMCS/O-HES hydrogel group.

Furthermore, from the H&E staining images of Figure 11, large amounts of proliferative cells or inflammatory cells were also detected in the process of wound healing. The inflammatory and proliferative cells were closely related to wound maturity. According to the scoring system of previous study, wound maturity was divided into five grades.[29] Grade 1 was no proliferative cells but highly inflammatory cells; grade 2 was mainly inflammatory cells; grade 3 was the same equivalence of inflammatory cells and proliferative cells; grade 4 was mainly proliferative cells; grade 5 was highly proliferative or even differentiated cells. From grade 1 to grade 5, the wound gradually matured. As indicated by the H&E and Masson's trichrome staining, on days 3 and 7 of wound healing, there were large amounts of inflammatory cells infiltrating into the upper layer of dermis and capillary vessels predominantly in the lower layer of dermis. On day 14, a new epidermal layer was formed and appeared upon the dermis layer. On days 14 and 21, the thickness of the epidermal layer was clearly observable, and there were mainly proliferative and even differentiated cells in the dermis layer. Simultaneously, newly formed collagen bundles were accumulated and deposited in the process of wound healing, as indicated by Masson's trichrome staining (Figure 12). The wound treated with M-CMCS/O-HES hydrogel and control group exhibited quick deposition of ECMs on day 7, especially for collagen stained as blue. After 10 days of wound healing, the collagen fibers were gradually decreased and arranged in an orientated pattern in both groups. In the later stages of healing from day 14 to day 21, the collagen fibers were decreased and replaced by the new regenerated skin appendages. Compared with the control group, the M-CMCS/O-HES hydrogel group showed more skin appendages of hair follicles, sweat glands, sebaceous glands, and vascular structures.

Quantitatively, the thickness of granulation tissue and regenerated epidermal layer and the extent of wound maturity and collagen deposition were also analyzed by histological evaluation. As indicated in Figure 13A, the thickness of granulation tissue in the M-CMCS/O-HES hydrogel group was significantly higher than that of the control group in the early stages of healing process (7, 10, and 14 days after

DOI: 10.1021/acsami.9b17180
ACS Appl. Mater. Interfaces 2020, 12, 2023−2038

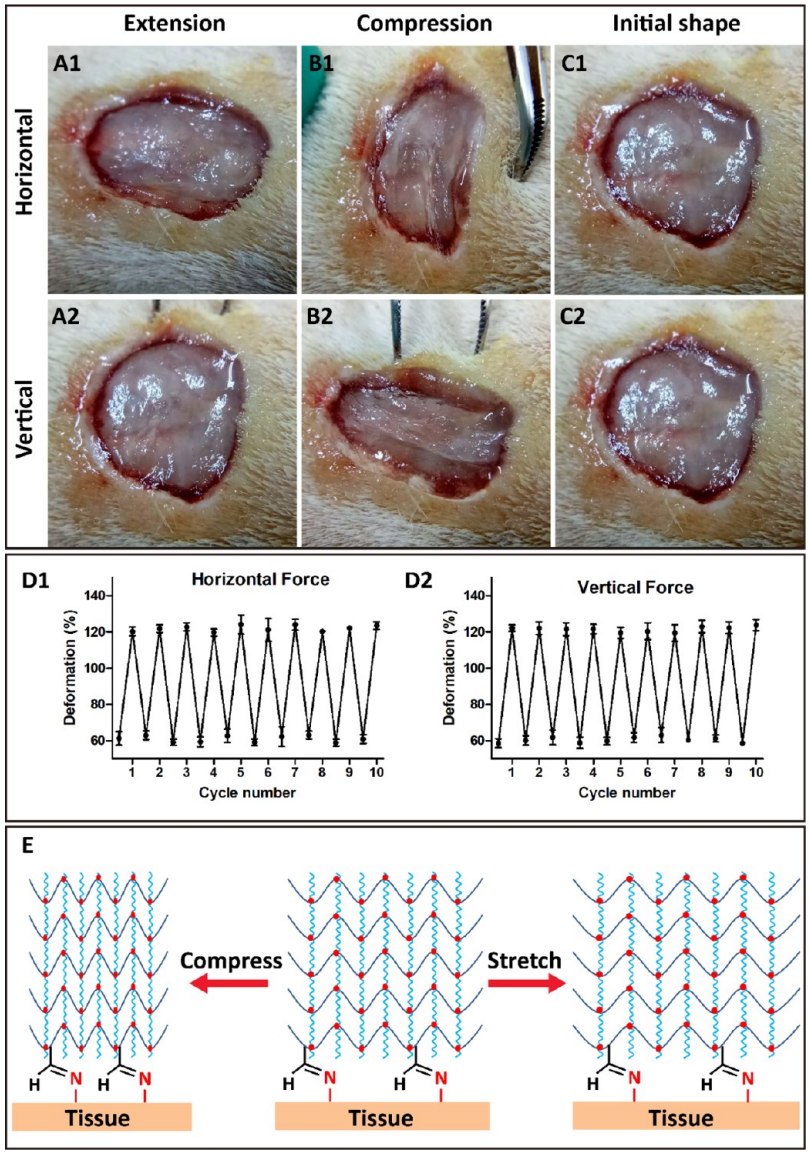

Figure 9. Self-recoverable compliance property of M-CMCS/O-HES hydrogel in vivo. Photographs of M-CMCS/O-HES hydrogel accommodating the skin movement of extension (A) and compression (B) and recovering original shape (C). Reversible extension and compression of M-CMCS/O-HES hydrogel under the horizontal force (D1) or vertical force (D2). (E) Schematic diagram of self-recoverable conformal contact deformation of M-CMCS/O-HES hydrogel during various skin movements.

surgery). Early in the process of wound healing, the formation of granulation tissue was advantageous for accelerating the wound repair. Furthermore, the thickness of the regenerated epidermal layer in the M-CMCS/O-HES hydrogel group was lower than that of the control group on days 14 and 21 (Figure 13B). In the previous studies,[30−32] the presence of hypertrophy of epidermis was considered as the main cause of adverse scar formation. Thus, the regenerated skin treated with M-CMCS/O-HES hydrogel showed a smaller scar area compared with the control group, indicating that the use of M-CMCS/O-HES hydrogel was conducive to the control of scar formation.

As for the extent of wound maturity, it was found that the M-CMCS/O-HES hydrogel group had a higher wound maturity score compared with that of the control group after 14 and 21 days (Figure 13C). In the early stages of healing process, the presence of collagen deposition was in favor of wound repair, whereas in the later stages of the healing process, the presence of large amounts of collagen increased scar deposition.[33] As shown in Figure 13D, the percentage of collagen deposition in the M-CMCS/O-HES hydrogel group was significantly higher than that of the control group on days 3, 7, 10 and 14. This was consistent with the faster wound closure treated with M-CMCS/O-HES hydrogel. After 21 days of skin regeneration, collagen deposition in the M-CMCS/O-HES hydrogel group was partially replaced by new regenerated skin appendages and lower than that of the control group. This was consistent with the smaller scar area observed in the M-CMCS/O-HES hydrogel group. Moreover, regenerated skin appendages obviously appeared in the dermis layer after 21 days when treated with M-CMCS/O-HES hydrogel, whereas no new skin appendages were formed in the control group. All of these results indicated that skin regeneration was enhanced by the use of M-CMCS/O-HES hydrogel. Therefore, M-CMCS/O-HES hydrogel was beneficial for promoting wound healing and improving the microstructure of regenerated skin.

DOI: 10.1021/acsami.9b17180
ACS Appl. Mater. Interfaces 2020, 12, 2023−2038

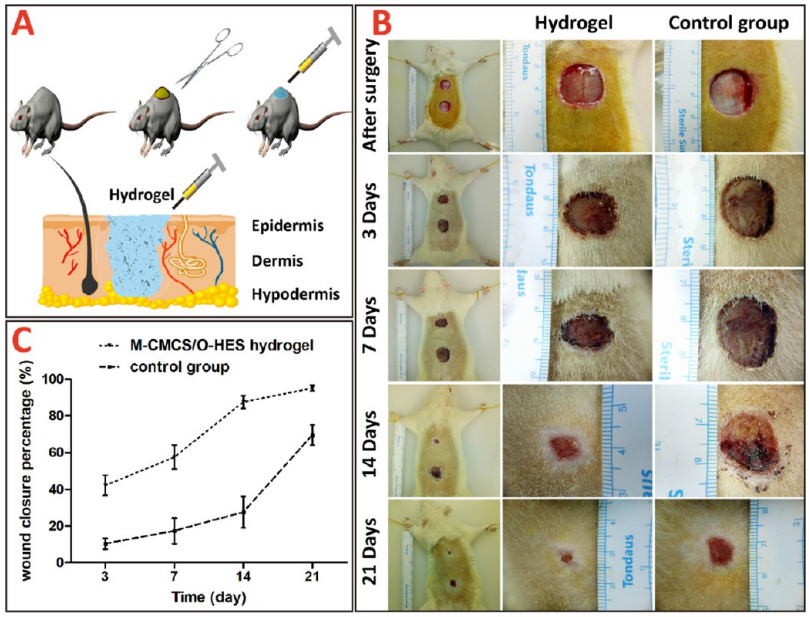

Figure 10. (A) Schematic diagram of full-thickness skin defects in SD rat model treated with M-CMCS/O-HES hydrogel. (B) Representative photographs of full-thickness skin defects treated with M-CMCS/O-HES hydrogel or not on days 0, 3, 7, 14, and 21 after surgery. (C) Quantitative analysis of wound closure in the M-CMCS/O-HES hydrogel group and control group. The results showed that wound closure percentage in the M-CMCS/O-HES hydrogel group was significantly higher than that in the control group on days 3, 7, 14, and 21 after surgery.

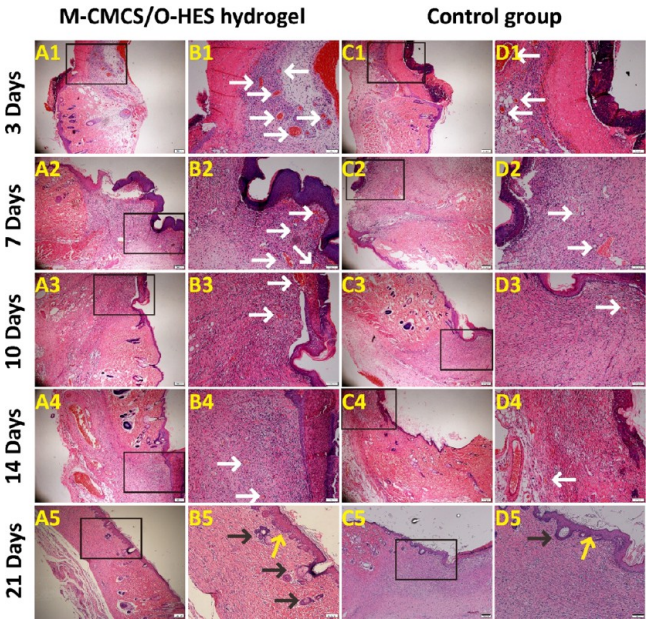

Figure 11. H&E staining analysis of regenerated skin tissue in the M-CMCS/O-HES hydrogel group (A,B) and control group (C,D) on days 3, 7, 10, 14, and 21 after surgery (white arrows: blood vessels; yellow arrows: epidermal layers; black arrows: hair follicles).

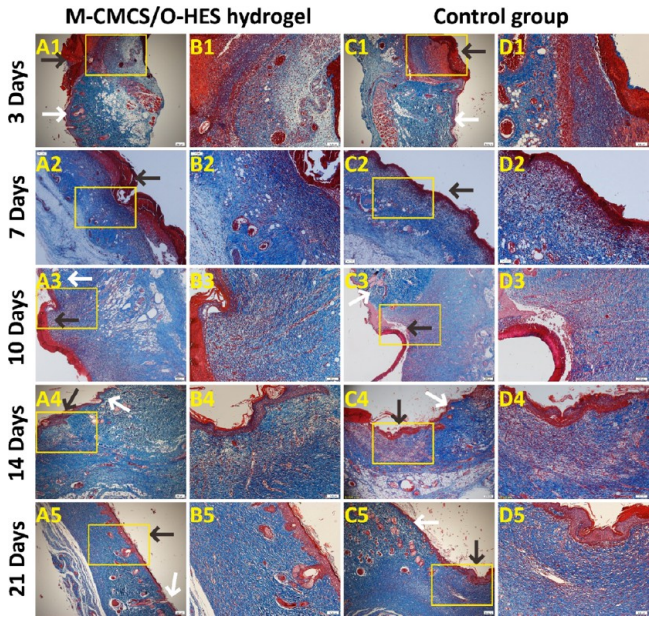

Figure 12. Masson's trichrome staining analysis of regenerated skin tissue in the M-CMCS/O-HES hydrogel group (A,B) and the control group (C,D) on days 3, 7, 10, 14, and 21 after surgery (white arrows: normal skin; black arrows: regenerated skin tissue).

4. DISCUSSION

In situ forming hydrogel scaffolds of various properties can be constructed by simply oxidizing HES and modifying CMCS according to this study. After mixing O-HES and M-CMCS solution, Schiff-based reaction takes place between −CHO and $-NH_2$ to form in situ hydrogels. Schiff-based reaction is a simple and fast cross-linking process that can occur at physiological pH and temperature without generation of heat and byproducts.[34] Using this technique, M-CMCS/O-HES hydrogels with gelation time in the range of 6−16 seconds and a swelling ratio of 15−40 have been made by varying processing parameters such as O-HES and M-CMCS volume fraction. This method also offers the independent control of porosity and pore size by varying the volume ratio of these two components. The ratio of these two components determines the final porosity and pore size distribution (50−200 μm) of the scaffolds. In this study, gelation time, equilibrium swelling performance, water-retaining capacity, and morphological characteristics of hydrogels have been studied extensively.

DOI: 10.1021/acsami.9b17180
ACS Appl. Mater. Interfaces 2020, 12, 2023−2038

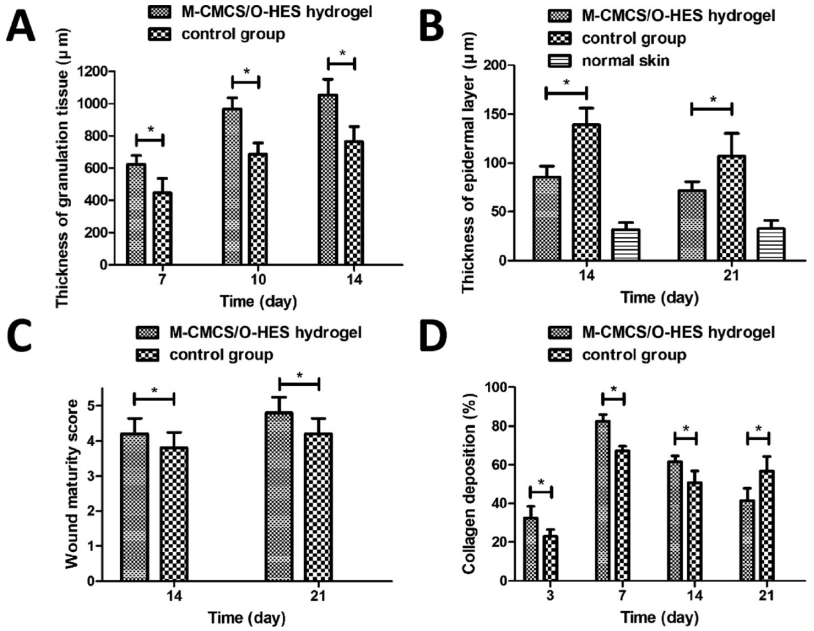

Figure 13. (A) Quantitative analysis of granulation tissue thickness in the M-CMCS/O-HES hydrogel group and control group on days 7, 10, and 14 after surgery. (B) Quantitative analysis of epidermal layer thickness in the M-CMCS/O-HES hydrogel group and control group on days 14 and 21 compared with the normal skin. (C) Quantitative assess of wound maturity in the M-CMCS/O-HES hydrogel group and control group on days 14 and 21 after surgery. (D) Statistics of collagen deposition in the M-CMCS/O-HES hydrogel group and control group on days 3, 7, 14, and 21 after surgery.

These properties of hydrogels are dependent upon the method of preparation, the polymer volume fraction, and the degree of cross-linking. If the specific requirements of these properties and biological performance for wound application can be fulfilled, M-CMCS/O-HES hydrogels are optimal biomaterial solution to accelerate wound healing.

As for wounds after traumatic injuries, the first and essential step is the immediate closure of wound, which not only promotes blood coagulation but also prevents the following potential infection.[1,35] Thus, immediate gelation is a prerequisite for injectable hydrogels to promote wound repair. After application, hydrogels must adhere to the wound site and completely seal the wound to prevent bacterial penetration, infection, and loss of body fluids. Moreover, they are required to gel and adhere to the wound even under moist conditions. In this study, injectability guarantees that the form of M-CMCS/O-HES hydrogels after gelation is consistent with the shape of skin defects. Rapid gelation ensures that the barrier of hydrogel can be formed immediately at the defect site to protect the wound from potential environmental hazards. Repeated stretching and compressing of M-CMCS/O-HES hydrogel in vivo endow it with self-recoverable compliance property to accommodate the wound under different states.

Because of the high water content, hydrogels are more inclined to resemble the natural ECM than any other type of polymeric biomaterials.[36] Researchers in the fields of hydrogels for biomedical applications prefer to use parameters to define the equilibrium-swelling behavior. For example, the so-called hydration ratio was introduced and calculated to evaluate the swelling behavior in some studies.[37−39] Meanwhile, another parameter of the weight degree of swelling was accepted by other researchers, which was defined as the ratio of the increased weight of the swollen sample to that of the dry sample.[40,41] In this study, the latter parameter was used to determine the equilibrium swelling and water-retaining capacity. M-CMCS/O-HES hydrogels have been demonstrated to absorb and contain large quantities of water, which successfully mimic the structure and property of ECM. Successful examples of in situ forming hydrogels include hyaluronan−gelatin[42] and collagen−hyaluronic acid hydrogels[43] used for promoting wound healing, which also displayed an exceedingly high water content in a fully swollen state.

This water uptake can lead to considerable swelling of hydrogel toward equilibrium. The degree of equilibrium swelling exerts an important effect on the diffusion of gas and nutrients into or out of the hydrogels. Generally, hydrogels that absorb large amounts of water exhibit high diffusion rates of molecules.[35] Furthermore, the pore size and porosity also influence the diffusion performance. In this study, the inherent porous and hydrophilic structure of M-CMCS/O-HES hydrogels guarantees gas exchange and fluid balance so as to support cell adhesion and proliferation. Moreover, the high water-retaining capacity assures them to trap wound exudates, control moisture evaporation, and then maintain a moist environment in the wound area. The advantages of a moist environment in the process of wound healing have been well documented, which can soften dry eschars, facilitate granulation tissue formation, favor angiogenesis, and promote reepithelialization.[44−47] By applying M-CMCS/O-HES hydrogels that reduce the loss of fluid, a moist environment can be created to accelerate wound healing.

Prior to the application of hydrogel scaffolds in animal models, their biological performance must also be evaluated to determine if they are biocompatible and will function in a biologically appropriate manner in the in vivo environment. These biological properties include biocompatibility and biodegradability under in vitro or in vivo conditions. The environment in vivo is a highly controllable biochemical reaction medium under normal conditions. The scaffolds in vivo are normally maintained in an isothermal (37 °C), neutral

DOI: 10.1021/acsami.9b17180
ACS Appl. Mater. Interfaces 2020, 12, 2023−2038

(pH 7.4), and aseptic aqueous environment. Through in vitro standards, these conditions appear to be mild and easy to simulate. In this study, in vitro biocompatibility and biodegradability tests were performed in a neutral and aseptic aqueous environment at 37 °C. Cell viability and proliferation depend on two simultaneous processes: nutrient substances migration into the hydrogels and metabolic waste diffusion outward through the swollen gels. As mentioned in the above results, M-CMCS/O-HES hydrogels support BMSC adhesion and proliferation during in vitro culture. However, the results of in vitro tests do not provide full information relevant to the in vivo situation. Thus, in vivo biocompatibility and biodegradability tests were also performed in this study.

As the constituents of M-CMCS/O-HES hydrogels are released into the body after degradation in vivo, the potential effect on host tissues and organs is also a concern. Because implanted scaffolds are replaced by the natural host tissue eventually, it is essential that the degradation products of the resorbable hydrogels must be composed of metabolically acceptable substances. M-CMCS/O-HES hydrogels derived from natural polysaccharides can be metabolized to CO_2 and H_2O and therefore are able to function for an appropriate time and then dissolve to disappear. As a result, M-CMCS/O-HES hydrogels show a low level of systemic toxicity because of their degradation to naturally occurring CO_2 and H_2O.

On the basis of physicochemical and biological assessments, M-CMCS/O-HES hydrogels combine many advantages for wound repair including biocompatibility, biodegradability, tunable porosity and pore size, high water-retaining capacity, ease of application in a moist environment for wound healing, barrier to protect the wound, and a potential matrix for cell or bioactive agent delivery. In the SD rat models of skin defects, M-CMCS/O-HES hydrogels serve as temporary skin substitutes. They provide a barrier to microbial invasion, help prevent fluid losses, and provide coverage while healing is taking place under the skin substitutes in vivo. It can be supposed that wound healing is enhanced by applying M-CMCS/O-HES hydrogels in the area of skin defects. This enhancement can be shown by higher wound closure percentage, more granulation tissue formation, faster epithelialization, and decreased collagen deposition. Taken together, the study confirms that in situ forming M-CMCS/O-HES hydrogels exhibited beneficial effects on wound healing and can be a promising therapeutic strategy for skin defects.

5. CONCLUSIONS

In this study, we prepared an in situ forming hydrogel with excellent self-recoverability, biocompatibility, biodegradability, and transparency to accelerate wound healing. O-HES was prepared by oxidizing HES with sodium periodate. The degree of oxidation was 74%. M-CMCS was prepared by grafting with ED. The amino content of M-CMCS was 0.53 mmol g^{-1}. M-CMCS/O-HES hydrogels with various ratios were investigated in vitro, and the best formulated M-CMCS/O-HES hydrogel was applied in vivo to accelerate wound healing. The results demonstrated that the physicochemical properties of M-CMCS/O-HES hydrogels through Schiff base reaction were dependent on the ratio of two components. M-CMCS/O-HES hydrogel with a volume ratio of 5:5 exhibited appropriate gelation time, notable water-retaining capacity, self-recoverable conformal deformation, suitable biodegradability, and good biocompatibility. Hence, this formulated M-CMCS/O-HES hydrogel was used to accelerate wound healing in SD rats. In comparison with the nontreatment control group, full-thickness skin defects treated with M-CMCS/O-HES hydrogel demonstrated higher wound closure percentage, more granulation tissue formation, faster epithelialization, and decreased collagen deposition. These findings suggest that the obtained M-CMCS/O-HES hydrogel is a promising therapeutic strategy for wound healing.

■ ASSOCIATED CONTENT

Supporting Information

The Supporting Information is available free of charge at https://pubs.acs.org/doi/10.1021/acsami.9b17180.

Repeated stretching and compressing of M-CMCS/O-HES hydrogel in vivo to verify self-recoverable conformal deformation property (MP4)

■ AUTHOR INFORMATION

Corresponding Authors

*E-mail: xmm@dhu.edu.cn (X.-M.M.).
*E-mail: chencheng@sspu.edu.cn (C.C.).
*E-mail: pansmith@163.com (J.-F.P.).

ORCID

Jun Li: 0000-0001-5027-1624
Xiu-Mei Mo: 0000-0001-9238-6171
Cheng Chen: 0000-0002-9813-532X

Author Contributions

J.L., F.Y., and G.C. contributed equally to this work.

Notes

The authors declare no competing financial interest.

■ ACKNOWLEDGMENTS

This work was financially supported by the National Natural Science Foundation of China (contract grant nos. 81802144 and 81901255) and the Fundamental Research Funds for the Central Universities (contract grant no. 22120180582) and the Research Project of Shanghai Municipal Population and Family Planning commission (contract grant no. 20164Y0050).

■ REFERENCES

(1) Singer, A. J.; Clark, R. A. F. Cutaneous Wound Healing. *N. Engl. J. Med.* **1999**, *341*, 738−746.
(2) Dreifke, M. B.; Jayasuriya, A. A.; Jayasuriya, A. C. Current Wound Healing Procedures and Potential Care. *Mater. Sci. Eng. C* **2015**, *48*, 651−662.
(3) Katzenell, U.; Ash, N.; Tapia, A. L.; Campino, G. A.; Glassberg, E. Analysis of the Causes of Death of Casualties in Field Military Setting. *Mil. Med.* **2012**, *177*, 1065−1068.
(4) Wei, G.; Ma, P. X. Nanostructured Biomaterials for Regeneration. *Adv. Funct. Mater.* **2008**, *18*, 3568−3582.
(5) Kim, E. J.; Choi, J. S.; Kim, J. S.; Choi, Y. C.; Cho, Y. W. Injectable and Thermosensitive Soluble Extracellular Matrix and Methylcellulose Hydrogels for Stem Cell Delivery in Skin Wounds. *Biomacromolecules* **2016**, *17*, 4−11.
(6) Zhang, K.; Bai, X.; Yuan, Z.; Cao, X.; Jiao, X.; Li, Y.; Qin, Y.; Wen, Y.; Zhang, X. Layered Nanofiber Sponge with an Improved Capacity for Promoting Blood Coagulation and Wound Healing. *Biomaterials* **2019**, *204*, 70−79.
(7) Jiang, J.; Carlson, M. A.; Teusink, M. J.; Wang, H.; MacEwan, M. R.; Xie, J. Expanding Two-Dimensional Electrospun Nanofiber Membranes in the Third Dimension by a Modified Gas-Foaming Technique. *ACS Biomater. Sci. Eng.* **2015**, *1*, 991−1001.

DOI: 10.1021/acsami.9b17180
ACS Appl. Mater. Interfaces 2020, 12, 2023−2038

(8) Guvendiren, M.; Molde, J.; Soares, R. M. D.; Kohn, J. Designing Biomaterials for 3d Printing. *ACS Biomater. Sci. Eng.* **2016**, *2*, 1679−1693.
(9) Kelly, C. N.; Miller, A. T.; Hollister, S. J.; Guldberg, R. E.; Gall, K. Design and Structure-Function Characterization of 3d Printed Synthetic Porous Biomaterials for Tissue Engineering. *Adv. Healthc. Mater.* **2018**, *7*, 1701095.
(10) Korting, H. C.; Schöllmann, C.; White, R. J. Management of Minor Acute Cutaneous Wounds: Importance of Wound Healing in a Moist Environment. *J. Eur. Acad. Dermatol. Venereol.* **2011**, *25*, 130−137.
(11) Winter, G. D. Formation of the Scab and the Rate of Epithelization of Superficial Wounds in the Skin of the Young Domestic Pig. *Nature* **1962**, *193*, 293−294.
(12) Hinman, C. D.; Maibach, H. Effect of Air Exposure and Occlusion on Experimental Human Skin Wounds. *Nature* **1963**, *200*, 377−378.
(13) Chouhan, D.; Lohe, T. U.; Samudrala, P. K.; Mandal, B. B. In Situ Forming Injectable Silk Fibroin Hydrogel Promotes Skin Regeneration in Full Thickness Burn Wounds. *Adv. Healthc. Mater.* **2018**, *7*, 1801092.
(14) Dimatteo, R.; Darling, N. J.; Segura, T. In Situ Forming Injectable Hydrogels for Drug Delivery and Wound Repair. *Adv. Drug Delivery Rev.* **2018**, *127*, 167−184.
(15) Liang, Y.; Zhao, X.; Hu, T.; Chen, B.; Yin, Z.; Ma, P. X.; Guo, B. Adhesive Hemostatic Conducting Injectable Composite Hydrogels with Sustained Drug Release and Photothermal Antibacterial Activity to Promote Full-Thickness Skin Regeneration During Wound Healing. *Small* **2019**, *15*, 1900046.
(16) Qu, J.; Zhao, X.; Liang, Y.; Zhang, T.; Ma, P. X.; Guo, B. Antibacterial Adhesive Injectable Hydrogels with Rapid Self-Healing, Extensibility and Compressibility as Wound Dressing for Joints Skin Wound Healing. *Biomaterials* **2018**, *183*, 185−199.
(17) Roy, C. K.; Guo, H. L.; Sun, T. L.; Ihsan, A. B.; Kurokawa, T.; Takahata, M.; Nonoyama, T.; Nakajima, T.; Gong, J. P. Self-Adjustable Adhesion of Polyampholyte Hydrogels. *Adv. Mater.* **2015**, *27*, 7344−7348.
(18) Zhao, X.; Wu, H.; Guo, B.; Dong, R.; Qiu, Y.; Ma, P. X. Antibacterial Anti-Oxidant Electroactive Injectable Hydrogel as Self-Healing Wound Dressing with Hemostasis and Adhesiveness for Cutaneous Wound Healing. *Biomaterials* **2017**, *122*, 34−47.
(19) Qu, J.; Zhao, X.; Ma, P. X.; Guo, B. Ph-Responsive Self-Healing Injectable Hydrogel Based on N-Carboxyethyl Chitosan for Hepatocellular Carcinoma Therapy. *Acta Biomater.* **2017**, *58*, 168−180.
(20) Dong, R.; Zhao, X.; Guo, B.; Ma, P. X. Self-Healing Conductive Injectable Hydrogels with Antibacterial Activity as Cell Delivery Carrier for Cardiac Cell Therapy. *ACS Appl. Mater. Interfaces* **2016**, *8*, 17138−17150.
(21) Upadhyaya, L.; Singh, J.; Agarwal, V.; Tewari, R. P. The Implications of Recent Advances in Carboxymethyl Chitosan Based Targeted Drug Delivery and Tissue Engineering Applications. *J. Control. Release* **2014**, *186*, 54−87.
(22) Zhao, X.; Li, P.; Guo, B.; Ma, P. X. Antibacterial and Conductive Injectable Hydrogels Based on Quaternized Chitosan-Graft-Polyaniline/Oxidized Dextran for Tissue Engineering. *Acta Biomater.* **2015**, *26*, 236−248.
(23) Liang, Y.; Zhao, X.; Hu, T.; Han, Y.; Guo, B. Mussel-Inspired, Antibacterial, Conductive, Antioxidant, Injectable Composite Hydrogel Wound Dressing to Promote the Regeneration of Infected Skin. *J. Colloid Interface Sci.* **2019**, *556*, 514−528.
(24) Qu, J.; Zhao, X.; Liang, Y.; Xu, Y.; Ma, P. X.; Guo, B. Degradable Conductive Injectable Hydrogels as Novel Antibacterial, Anti-Oxidant Wound Dressings for Wound Healing. *Chem. Eng. J.* **2019**, *362*, 548−560.
(25) Tomihata, K.; Ikada, Y. In vitro and in vivo degradation of films of chitin and its deacetylated derivatives. *Biomaterials* **1997**, *18*, 567−575.
(26) Lu, G.; Kong, L.; Sheng, B.; Wang, G.; Gong, Y.; Zhang, X. Degradation of Covalently Cross-Linked Carboxymethyl Chitosan and Its Potential Application for Peripheral Nerve Regeneration. *Eur. Polym. J.* **2007**, *43*, 3807−3818.
(27) Lu, G.; Sheng, B.; Wang, G.; Wei, Y.; Gong, Y.; Zhang, X. Controlling the Degradation of Covalently Cross-Linked Carboxymethyl Chitosan Utilizing Bimodal Molecular Weight Distribution. *J. Biomater. Appl.* **2009**, *23*, 435−451.
(28) Saghazadeh, S.; Rinoldi, C.; Schot, M.; Kashaf, S. S.; Sharifi, F.; Jalilian, E.; Nuutila, K.; Giatsidis, G.; Mostafalu, P.; Derakhshandeh, H.; Yue, K.; Swieszkowski, W.; Memic, A.; Tamayol, A.; Khademhosseini, A. Drug Delivery Systems and Materials for Wound Healing Applications. *Adv. Drug Delivery Rev.* **2018**, *127*, 138−166.
(29) Milan, P. B.; Lotfibakhshaiesh, N.; Joghataie, M. T.; Ai, J.; Pazouki, A.; Kaplan, D. L.; Kargozar, S.; Amini, N.; Hamblin, M. R.; Mozafari, M.; Samadikuchaksaraei, A. Accelerated Wound Healing in a Diabetic Rat Model Using Decellularized Dermal Matrix and Human Umbilical Cord Perivascular Cells. *Acta Biomater.* **2016**, *45*, 234−246.
(30) van den Broek, L. J.; Limandjaja, G. C.; Niessen, F. B.; Gibbs, S. Human Hypertrophic and Keloid Scar Models: Principles, Limitations and Future Challenges from a Tissue Engineering Perspective. *Exp. Dermatol.* **2014**, *23*, 382−386.
(31) Yang, S.-w.; Geng, Z.-j.; Ma, K.; Sun, X.-y.; Fu, X.-b. Comparison of the Histological Morphology between Normal Skin and Scar Tissue. *J. Huazhong Univ. Sci. Technol., Med. Sci.* **2016**, *36*, 265−269.
(32) Tandara, A. A.; Mustoe, T. A. The Role of the Epidermis in the Control of Scarring: Evidence for Mechanism of Action for Silicone Gel. *J. Plast. Reconstr. Aesthet. Surg.* **2008**, *61*, 1219−1225.
(33) Volk, S. W.; Wang, Y.; Mauldin, E. A.; Liechty, K. W.; Adams, S. L. Diminished Type Iii Collagen Promotes Myofibroblast Differentiation and Increases Scar Deposition in Cutaneous Wound Healing. *Cells Tissues Organs* **2011**, *194*, 25−37.
(34) Jia, Y.; Li, J. Molecular Assembly of Schiff Base Interactions: Construction and Application. *Chem. Rev.* **2015**, *115*, 1597−1621.
(35) Ghobril, C.; Grinstaff, M. W. The Chemistry and Engineering of Polymeric Hydrogel Adhesives for Wound Closure: A Tutorial. *Chem. Soc. Rev.* **2015**, *44*, 1820−1835.
(36) Zhu, J.; Marchant, R. E. Design Properties of Hydrogel Tissue-Engineering Scaffolds. *Expert Rev. Med. Devices* **2011**, *8*, 607−626.
(37) Fang, J.-Y.; Chen, J.-P.; Leu, Y.-L.; Hu, J.-W. The Delivery of Platinum Drugs from Thermosensitive Hydrogels Containing Different Ratios of Chitosan. *Drug Deliv.* **2008**, *15*, 235−243.
(38) Noble, L.; Gray, A. I.; Sadiq, L.; Uchegbu, I. F. A Non-Covalently Cross-Linked Chitosan Based Hydrogel. *Int. J. Pharm.* **1999**, *192*, 173−182.
(39) Wei, Y. T.; Tian, W. M.; Yu, X.; Cui, F. Z.; Hou, S. P.; Xu, Q. Y.; Lee, I.-S. Hyaluronic Acid Hydrogels with Ikvav Peptides for Tissue Repair and Axonal Regeneration in an Injured Rat Brain. *Biomed. Mater.* **2007**, *2*, S142−S146.
(40) Lueckgen, A.; Garske, D. S.; Ellinghaus, A.; Desai, R. M.; Stafford, A. G.; Mooney, D. J.; Duda, G. N.; Cipitria, A. Hydrolytically-Degradable Click-Crosslinked Alginate Hydrogels. *Biomaterials* **2018**, *181*, 189−198.
(41) Namazi, H.; Hasani, M.; Yadollahi, M. Antibacterial Oxidized Starch/Zno Nanocomposite Hydrogel: Synthesis and Evaluation of Its Swelling Behaviours in Various Phs and Salt Solutions. *Int. J. Biol. Macromol.* **2019**, *126*, 578−584.
(42) Qin, X.; Qiao, W.; Wang, Y.; Li, T.; Li, X.; Gong, T.; Zhang, Z.-R.; Fu, Y. An Extracellular Matrix-Mimicking Hydrogel for Full Thickness Wound Healing in Diabetic Mice. *Macromol. Biosci.* **2018**, *18*, 1800047.
(43) Ying, H.; Zhou, J.; Wang, M.; Su, D.; Ma, Q.; Lv, G.; Chen, J. In Situ Formed Collagen-Hyaluronic Acid Hydrogel as Biomimetic Dressing for Promoting Spontaneous Wound Healing. *Mater. Sci. Eng., C* **2019**, *101*, 487−498.

DOI: 10.1021/acsami.9b17180
ACS Appl. Mater. Interfaces 2020, 12, 2023−2038

(44) Atiyeh, B.; Ioannovich, J.; Al-Amm, C.; El-Musa, K. Management of Acute and Chronic Open Wounds: The Importance of Moist Environment in Optimal Wound Healing. *Curr. Pharmaceut. Biotechnol.* **2002**, *3*, 179−195.
(45) Bolton, L. Operational Definition of Moist Wound Healing. *J. Wound, Ostomy Cont. Nurs.* **2007**, *34*, 23−29.
(46) Wiechula, R. The Use of Moist Wound-Healing Dressings in the Management of Split-Thickness Skin Graft Donor Sites: A Systematic Review. *Int. J. Nurs. Pract.* **2003**, *9*, S9−S17.
(47) Singer, A. J.; Dagum, A. B. Current Management of Acute Cutaneous Wounds. *N. Engl. J. Med.* **2008**, *359*, 1037−1046.

DOI: 10.1021/acsami.9b17180
ACS Appl. Mater. Interfaces 2020, 12, 2023−2038